SI Appendix

1. Lateral and vertical carbon fluxes induced by erosion

1.1 Lateral carbon fluxes (F1 and F2)

1.1.1 Soil Organic Carbon (SOC) erosion (F1)

The erosional component of soil organic carbon (SOC) was derived using the following equation:

$$E_C = C_{SOC-Surf} v_{ero} A_{ero} \quad (1)$$

where E_C (kg/yr) is the amount of organic carbon loss due to soil erosion, $C_{SOC\text{-}surf}$ (kg/m^3) is the organic carbon content in the surficial soil layer of 4.5 cm (see Section 2.2 for soil data format), v_{ero} (m/yr) is the water erosion rate, and A_{ero} (m^2) is the erosional area. This approach assumes that the enrichment ratio $E_r = 1$. In other words it is assumed that the proportion of SOC in the soil is the same as that which is eroded and therefore transported away from the eroded site. We recognize that there are situations in which $Er > 1$ and that the amount of SOC eroded is larger than the SOC content because SOC is removed preferentially. However, there is little data presently available with which to parameterize our model.

1.1.2 SOC deposition (F2)

The SOC depositional component was similarly assessed from:

$$D_C = C_{SOC-Surf} v_{dep} A_{dep} \quad (2)$$

where D_C (kg/yr) is the amount of organic carbon loss due to soil erosion, v_{dep} (m/yr) is the deposition rate, and A_{dep} (m^2) is the depositional area. We assume that there is no preferential sorting of material and that all of the eroded SOC is deposited at the same location.

Sediment Delivery Ratio (*SDR*) is defined as the ratio of sediment transport (T_S, kg/yr) to the total amount of soil erosion (E_S, kg/yr):

$$SDR = \frac{T_S}{E_S} \quad (3)$$

Since deposition is the difference between soil erosion and sediment transport, and the enrichment ratio is assumed to be 1, equation (2) can be converted into:

$$D_C = E_C \cdot (1 - SDR) \quad (4)$$

Based on observations of *SDR* in nine major river basins in China, Jing et al. (1) established a positive relationship between the five grades of soil erosion severity and *SDR* in the range 0.1–1 throughout China at the scale of small watersheds (~1 km^2) (Table S3). This positive relationship is mainly due to the feedback of sediment delivery on soil erosion: with smaller *SDR*, more sediment accumulates within its source watershed, which would prohibit further erosion as the depositional area approaches full capacity. The observed *SDR* values and erosion grades in other representative areas have also been collected from various sources in the literature to support the relationship obtained by Jing et al. (1) (Table S4). Thus, the magnitude of SOC deposition in all cells (polygons) can be calculated using equation (4).

1.1.3 Validation of lateral carbon fluxes

Data concerning SOC removal and deposition in small watersheds have been collected to validate the modeled F1 and F2 in this paper. Table S5 shows that the values of F1 and F2 agree well with those from previous studies carried out in different regions of China.

1.2 Carbon recovery at the eroded area (F3)

1.2.1 Identifying the erosion-induced CO_2 fluxes in small watersheds

Van Oost et al. (2) designed a novel method to separate the component of CO_2 flux that is solely induced by soil erosion in small watersheds. According to Schmidt et al. (3), the molecular structure of Soil Organic Matter (SOM) plays a secondary role in determining the carbon decomposition and persistence, and the ecosystem properties (i.e. biotic and abiotic environments) determine the carbon stability. Furthermore, the biochemical decomposition and persistence are far from equilibrium, especially in the eroding area (4). To quantify the CO_2 exchange induced by soil erosion in the eroding area, Van Oost et al. (2) first assume an equivalent situation between biochemical composition and decomposition, and simulate the change of SOC (ΔC_{sim}, g C/m^2); then by subtraction from the observed SOC content (ΔC_{obs}, g C/m^2), Van Oost et al. (2) estimate the carbon exchange induced by other environmental variables (primarily soil erosion) as the dynamic recovery:

$$F3 = (\Delta C_{obs} - \Delta C_{sim}) / T \tag{5}$$

in which ΔC_{obs} is regarded as the difference between the initial carbon stock C_0 (g C/m^2) and that after T years, $C_{T\text{-}E}$ (g C/m^2):

$$\Delta C_{obs} = C_{T-E} - C_0 \tag{6}$$

Note that ΔC_{sim} is determined through mathematical simulation of the evolution of stock during the process of soil erosion without extra CO_2 exchange induced by erosion. ΔC_{sim} is divided into two parts: (1) $F_{con\text{-}de}$ (g C/m^2; *con* stands for composition, and *de* stands for decomposition), the carbon changes due to composition/decomposition of SOC under stable conditions (i.e. without erosion), and (2) $F_{ero\text{-}l}$ (g C/m^2; *l* stands for lateral), lateral carbon loss due to erosion, excluding a component reflecting the interaction between soil erosion and CO_2 emission/sequestration:

$$\Delta C_{sim} = F_{con-de} + F_{ero-l} \tag{7}$$

By subtracting ΔC_{sim} from ΔC_{obs}, the erosion-induced CO_2 exchange is quantified. In non-eroded areas, changes to soil carbon storage are caused by biochemical composition and decomposition of organic carbon. Therefore, $F_{con\text{-}de}$ can be calculated as the difference between initial carbon storage and carbon stock during the T-th year within the stable area of a watershed $C_{T\text{-}NE}$ (g C/m^2):

$$F_{con-de} = C_{T-NE} - C_0 \qquad (8)$$

Lateral carbon movement due to soil erosion $F_{ero\text{-}l}$ can be calculated in terms of erosion rate v_{ero} (m/yr), duration of erosion period T (yr), and carbon content in the top layer directly affected by soil erosion (~20 cm) in the t-th year, $c_{top(t)}$ (g C/m^3) , i.e.,

$$F_{ero\text{-}l} = \sum_{t=1}^{T} v_{ero} c_{top(t)} \qquad (9)$$

Combining equations (1) to (9), the total erosion-induced CO_2 flux during T years, $F_{ero\text{-}v}$ (g C/m^2; v stands for vertical), can be calculated according to:

$$F_{ero-v} = C_{T-E} - C_{T-NE} - \sum_{t=1}^{T} v_{ero} c_{top(t)} \qquad (10)$$

Note that $c_{top(t)}$ changes with time:

$$c_{top(t)} = \frac{c_{top(t-1)} D_{top} + (c_{bel(t-1)} - c_{top(t-1)}) v_{ero}}{D_{top}} \qquad (11)$$

The parameters $C_{T\text{-}E}$, $C_{T\text{-}NE}$, $c_{top(t)}$, $c_{top(t\text{-}1)}$, $c_{bel(t\text{-}1)}$ and D_{top} are determined from the vertical profiles of organic carbon in both stable and erosional areas of the watershed. v_{ero} is derived from the ^{137}Cs content in soil profiles. Therefore, the annual erosion-induced CO_2 source/sink across the whole watershed during erosion period T (yr), $F3$ (g C/yr), is:

$$F3 = (\sum_{i=1}^{N} F_{ero-v(i)} A_{(i)}) / T \quad (12)$$

where N is the number of soil samples in the watershed, and $A_{(i)}$ is the controlling area of the i-th sample.

Using the above method, Van Oost et al. (2) successfully determined erosion-induced CO_2 fluxes in small basins. Since discrimination is needed between stable and erosional areas in a given watershed over the years of erosion history, it is difficult to upscale the method to other, larger regions lacking such information. Moreover, the use of ^{137}Cs to determine erosion velocities is too expensive to implement in larger regions. Although the mapping of ^{137}Cs data and the estimation of net soil redistribution is possible over large areas (5, 6), we took a modelling approach to tackle this problem across China.

1.2.2 Improved Method

A key problem in the assessment of erosion-induced CO_2 fluxes in large-scale basins arises from data availability. A modified approach is thus needed to avoid the necessity for discrimination between stable and erosional areas. Moreover, alternatives are needed for determination of erosion rates.

Instead of choosing the first year since erosion as the beginning of the simulation period, the N-th year after erosion is selected as the start point (Fig. S1). Similarly we assume that erosion does not exert any impact on the original CO_2 exchange process, soil carbon composition/decomposition and lateral movement of organic carbon are simulated as two independent processes, with the modeled carbon storage being C_{unc} (g C/m^2). Then, the coupled carbon storage (C_{coup}, g C/m^2) is modeled including the impact of erosion on CO_2 emission/sequestration (Fig. S1). The difference in carbon storage under the two circumstances is regarded as the erosion-induced CO_2 flux in the erosional area, $F3$ (g C/yr). The parameters C_{unc}, C_{coup} and F3 are obtained respectively from:

$$\frac{dC_{unc}}{dt} = I_B - k_O C_{unc} \tag{13}$$

$$\frac{dC_{coup}}{dt} = I_B - (k_O + k_E) C_{coup} + c_{bel} v_{ero} \tag{14}$$

and

$$F3 = \frac{C_{coup} - C_{unc}}{T} A_{ero} \,. \tag{15}$$

It should be noted that C_{coup} and C_{unc} are the carbon contents within corresponding layers in the original soil profile. In Equations (13)~(15), I_B (g C/m^2/yr) is the carbon input to the soil, and k_O (1/yr) is the turnover rate of soil carbon with respect to decomposition in absence of erosion. k_E (1/yr) is the erosion rate of soil carbon, obtained by calculating the ratio of soil erosion rate (m/yr) to the depth of carbon in the top soil layer which dominates erosion. Both C_{coup} and C_{unc} are effectively carbon storages in the top layers, considering that there is no difference in the coupled and uncoupled carbon storages in the deeper layers. These levels are seldom affected by soil erosion, and provide no contribution to the erosion-induced CO_2 sink from the deeper layers. c_{bel} (g C/m^3) is the carbon concentration at the bottom of the top layer. Since the vertical distribution of organic carbon usually obeys an exponential law, c_{bel}, is expressed:

$$c_{bel} = (c_0 - c_{\min}) e^{-k v_{ero} t} + c_{\min} \tag{16}$$

where c_0 (g C/m^3), c_{min} (g C/m^3), and k (1/m) can be determined by measurements of carbon concentration in different layers of vertical soil profiles. c_0 is averaged over the whole top layer (therefore uniform within the top layer, and is equal to C_{bel} when t = 0). Dividing all terms in equation (16) by c_0, then:

$$\frac{c_{bel}}{c_0} = \frac{c_{\min}}{c_0} + \left(1 - \frac{c_{\min}}{c_0}\right) e^{-k v_{ero} t} \tag{17}$$

We then divide $\frac{c_{\min}}{c_0}$ in the range of 0.01–0.5 using an incremental step of 0.01. Then, for each $\left(\frac{c_{\min}}{c_0}\right)_i$ (i = 1 … 50), the measured carbon concentration is fitted to the l layers of samples: $\left(\frac{cz_j}{c_0}, z_j\right)_{ref}$ (j = 1 … l), and the best-fit k_i parameterized using the least squares method. From all 50 pairs of $\left(\frac{c_{\min}}{c_0}, k\right)_i$, the case is selected that leads to the minimum root-mean-square-error (RMSE), which is usually less than 40%. For the thin soil layer, $\frac{c_{\min}}{c_0}$ is set to 0.01. Fig. S2 illustrates the entire parameterization process. A_{ero} and T in equation (15) represent the erosional area of the studied watershed and the length of the simulation period, respectively.

Berhe et al. (7) used a humification coefficient to evaluate the fraction of net primary production (NPP) entering into the soil, with the remainder of NPP assumed to be rapidly decomposed and released to the atmosphere without participating in the processes of soil erosion and terrestrial deposition. To apply this method, an estimate of humification coefficient is required. However, little information about the humification coefficient is available for different ecosystem types in China. The approach taken herein assumes that all NPP enters the soil carbon pool (i.e. I_B = NPP), and considers the uncertainty by using a k_O already including the initial rapid carbon loss, which is different to that of Berhe et al. (7). In Section 3, different values for the humification coefficient (< 10% in grasslands and forests, and < 30% in agricultural systems) have been assumed to analyze the uncertainty. Moreover, the "initial rapid C loss" hypothesis should be viewed with caution because newly produced photosynthate may become invulnerable to rapid decomposition under certain circumstances including physical protection (e.g. soil burial, waterlogging). In such cases, the photosynthate may become a C substrate for soil erosion, i.e. NPP. It should be noted that as SOC declines due to continuous erosion, and k_O from these models could be over-estimated (8). The sensitivity of k_O is tested in Section 3. We also assume that erosion has no effect on the rate of SOC decomposition, and the related uncertainty is discussed in Section 3.

Since NPP is linearly dependent on crop yield, such that

$$\mathrm{NPP} = \frac{CropYield}{HI} \quad DF \quad CF , \tag{18}$$

where HI is the Harvest Index, DF is the Dry matter Fraction, and CF is the Carbon

Fraction. The increase in crop yield per unit area recorded in all provinces (Table S6) implies that NPP was maintained even under severe soil erosion. Therefore, it is reasonable to assume that NPP is slightly affected by soil erosion, even in severely eroded areas like the Loess Plateau (9) and Southwest China (10).

Using equations (13) to (17), the erosion-induced CO_2 fluxes are determined from the storage and vertical profile of soil organic carbon, erosion rate, carbon pool turnover rate, and net primary production (NPP).

The modified method simplifies the discrimination of stable and erosional areas, and avoids having to estimate the year in which erosion commenced. Moreover, the majority of model inputs such as erosion rate, soil carbon storage, carbon pool turnover rate and NPP can be extracted from either national survey databases or global carbon cycle models. Comparison of data requirements for the two methods (Table S7) shows closer data accessibility by the modified method for assessment at regional scale. It should also be noted that the modified method does not take into account the DOC leaching term, which could contribute another source of vertical carbon loss. This uncertainly will also be discussed in Section 3.

1.2.3 Scale-up approach based on minimum polygons

Although estimation of dynamic replacement can be undertaken at the scale of small watersheds using the modified method, estimation over larger regions remains a problem. Scale-up from local to regional scales is a key issue in extrapolation to large areas. Here we propose an efficient approach based on minimum polygons identified as continuous small areas with uniformly distributed geographical factors (11, 12), such as soil organic carbon content, erosion grade, carbon pool turnover rate, and NPP. By overlaying these factors at different layers (Table S8) in GIS software (Fig. S3), tens of thousands of polygons are generated, the majority of which have areas less than 1 km^2. Thus, the total erosion-induced CO_2 sequestration can be obtained by summing up the CO_2 fluxes in each of the polygons.

1.2.4 Comparison between Van Oost et al.'s (2) and modified methods

Since it is difficult to observe the CO_2 flux induced by erosion in small watersheds, we test the modified method by comparing its outputs with those from Van Oost et al.'s (2) method for 8 watersheds in Europe, 2 watersheds in the US, and 5 watersheds in China. The ^{137}Cs and SOC data for watersheds in Europe and the US are taken from the Supplementary Material of Van Oost et al. (2). The 5 representative small watersheds in China are located in the black soil region, the red soil region, and the purple soil region. The spatial distribution of soils in China is shown in Fig. S4. Watershed No.1, with an area of 13 ha, is located in the black soil area of Jilin Province (125°52′E, 44°43′N) which has a cold (average temperature: 4.4°C), humid (annual precipitation: 534 mm) climate. Under the influence of the continental monsoon, 70% of the precipitation occurs between June and August. Watershed No.1 is severely eroded because of the long cultivation history of corn dating back to 1903, noting that the cultivation depth is about 20 cm (13). Watershed No.2 is located in the black soil area of Heilongjiang Province with average temperature of 0.5–4.0 °C and humid climate (mean annual precipitation of 500–600 mm). Under the influence of the continental monsoon, 80% of the precipitation is concentrated from June to September. Bean is the main crop in this region (14). However, Watersheds No.3 and No.4 are all within Jianyang County (104°28′E, 30°26′N) in the eastern part of Sichuan Basin and comprise purple soil which is cultivated by rotating wheat, corn and potato crops (15, 16). These two watersheds are characterized by very hilly topography (average slope of 16%) and relatively low altitude (400–587 m), and their climate is hot and humid with average temperature of 17.4°C and annual precipitation of 872 mm. Watershed No.5 is covered by red soil containing relatively little organic matter, located in the Liujiashan Farm (109°20′E, 33°44′N) in Yujiang County, Jiangxi Province. This watershed is characterized by low (altitude: 45–60 m), hilly (slope: 5–18%) topography. The average temperature is 17.8°C. The annual precipitation is 1795 mm, 50% of which occurs in the monsoon season from April to June. The main crops are tea, peanuts, and carrots, which have been cultivated since the 1950s (17).

Table S9 lists the collected SOC and ^{137}Cs data together with the relevant parameters reported in the literature for the 15 test watersheds. Comparison of outputs from both Van Oost et al.'s (2) and the present modified model are given in Table S9 and Fig. S1. The RMSE for the Chinese watersheds in China is 19.3%, and that for other watersheds is 39.7%. The average RMSE for the total is 31.7 %. Although the tested watersheds are widely distributed in Europe, the US, and China, the total number of basins considered is small in terms of statistical significance, and more *in situ* data are needed in future. To further test the modified method, a sensitivity analysis is reported in Section 3.

1.3 Erosion-induced CO_2 source in the depositional area (F4)

It is commonly accepted that erosion induces a CO_2 source in the depositional area (18, 19). As the eroded soil is deposited, part of the top soil layer enters into the 1st layer of sub-soil (19). Therefore, the depth of the layer next to the top layer becomes thick. Decomposition of the newly buried C-rich soil brings about an extra CO_2 source. Thus, F4 can be calculated based on the total eroded soil of the polygon:

$$F4 = C_{SOC\text{-}\mathrm{surf}}\,\bar{v}_{ero}\,k_{O\text{-}subsoil}(1 - SDR) \quad (19)$$

where $\bar{v}_{ero}$ is the mean erosion rate of the polygon (i.e. $v_{ero}A_{ero}/A_{polygon}$; and $A_{polygon}$ is the area of the polygon); $k_{O\text{-}subsoil}$ is the turnover rate of the subsoil layer; *SDR* is a conceptual parameter defined as the ratio of the total sediment exported out of the polygon to the total eroded soil within the polygon. Since the turnover rate decreases exponentially with depth (19):

$$k_{o-z} = k_{o-0}\exp(-u_r z) \quad (20)$$

where u_r is set to 2.6, the decomposition rate of the newly buried SOC is 40–60 % of the top layer, noting that z is usually within the range of 0.2–0.3 m.

Although the assumption of exponential decay is more acceptable close to steady state conditions, the rate of decay of the soil C reservoir is no longer exponential in a depositional landform associated with grassland that is naturally eroding (7). Nevertheless, buried SOC remains conserved over the decadal time period considered herein, as found by Van Oost et al. (2, 20) and Wang et al. (21). This is because the decay rates diminish substantially in burial zones, with the primary control factor provided by the physical environment, not the SOC chemistry. Hence, it is reasonable to use an exponential decay law.

1.4 Enhanced decomposition of SOC during sediment transport (F5)

Soil aggregates detach during erosion, and break down further when delivered to depositional land, making it easier to decompose organic carbon in sediments. Meanwhile, the presence of autochthonous carbon in the aquatic environment enhances SOC mineralization. Unlike Jacinthe et al. (22) who reported that up to 50% SOC degraded into CO_2 in an incubation experiment lasting 100 days, Wang et al. (21) found that hardly any additional CO_2 was released owing to erosion. Following Guenet et al. (23) we assume that the difference between decomposition *in situ* and during transport could be as much as 63%. Here, we evaluate the erosion-induced CO_2 flux during sediment transport by assuming that 63% more SOC is degraded into CO_2 in water than in the soil layers. Other studies have also reported that the additional emission is very small (e.g. Van Hemelryck et al., 24). Hence, the approach taken herein is consistent with the understanding of erosional effects on decomposition rates on land.

1.5 VLC Ratio

The Vertical to Lateral Carbon (VLC) ratio is defined as the ratio of the recovery CO_2 sink (F3) to SOC removal (F1) in eroding areas. VLC reflects the potential of a certain area to recover from the loss of SOC.

2. Data

2.1 National Survey on Soil Erosion

Two detailed national soil erosion surveys were accomplished in 1995–1996 and 2010–2012, and the data can be downloaded from (http://cese.pku.edu.cn/chinaerosion/). The first national survey combined remote sensing (TM) images and field survey data to provide spatial distribution information on primary geographical and environmental factors such as erosive force, topography and vegetation. As a result, six soil erosion grades were classified over the entire country (25) (Fig. S5). Furthermore, the second national survey utilized Chinese Soil Loss equation (26) (CSLE), with inputs of topographical, land use and remote-sensing information as well as field survey data on conservation measures, vegetation cover and meteorology (32,364 small watersheds covering 1% of the water erosion area in China). Erosion rates were calculated from:

$$A = R \cdot K \cdot L \cdot S \cdot B \cdot E \cdot T \ . \tag{21}$$

where A is the erosion rate (t/hm^2/yr), R is the rainfall erosivity (MJ mm/hm^{2}ha), K, the soil erodibility index, refers to the soil loss of a unit plot that is 22.1 m long and 9 % steep (unit: t hm^2 h/hm^2 JM mm), L is the slope length factor (-), S is the slope factor (-), B is the biological conservation measures factor, E is the engineering conservation measures factor, and T is the tillage conservation measures factor. R appears in terms of the average rainfall-erosivity over 24 half-months, i.e. R_{hm} (MJ mm/hm^{2}ha):

$$R_{hm} = 0.184 \sum_{i=1}^{n} (P_d I_{10d})_i \tag{22}$$

where P_d is the daily rainfall amount (mm) and I_{10d} is the daily maximum 10min rainfall intensity (mm/h). K is estimated according to its definition above (Fig. S6(a)).

In equation (21), L is determined from:

$$L = (\lambda / 22.13)^m \tag{23}$$

where λ is the slope-length (m) and m is the slope length exponent identified as:

$$m = 0.6(1 - e^{-35.835 \tan\theta}) \tag{24}$$

S is determined from:

$$S=\begin{cases}10.8\sin\theta+0.03 & \theta\le 5^{\circ}\\ 16.8\sin\theta-0.5 & \theta>5^{\circ}\end{cases} \tag{25}$$

where θ is the slope gradient.

E is expressed as:

$$E=(1-\frac{s_t}{s_0}a)(1-\frac{s_d}{s_0}b) \tag{26}$$

where s_t is the area of terraces (km^2); s_d is the control area of check dams (km^2); s_0 is the area of sub-basins (km^2); and *a* and *b* are sediment-reduction coefficients associated with terraces and check dams.

B and *T* are obtained from:

$$B=\sum_{i=1}^{n}M_i/M_{0i}, \quad T=\sum_{i=1}^{n}M_i/M_{0i} \tag{27}$$

where M_i (t/hm^2) is the soil loss under certain conservation measures in the *i*-th year, and M_{0i} (t/hm^2) is the soil loss of a bare field in the *i*-th year. For easier application, the factor *B* is often determined according to land-use type and vegetation cover (27). Table S10 lists references to the validation of CSLE for watersheds in different regions of China.

Precipitation is a key parameter affecting soil erosion. Two different series of climate data are chosen for corresponding calculations based on national surveys undertaken in 1995–1996 and 2010–2012. According to equations (1–2, 19), F1, F2, F4, and F5 are linearly dependent on erosion rate, and F3 also has a positive correlation with erosion rate (see sensitivity analysis in Section 3). Therefore, the weighting of climate on the five carbon fluxes can be reflected by its impact on erosion rate. Miao et al. (28) suggest that climate change contributes 17% and 48% of the decrease of sediment yield in the upper and middle reaches of Yellow River Basin, respectively.

Considering that uncertainties exist in both the sources of data (DEM, survey on *B*, *E*, and *T* factors) and the model employed, the national surveys reported soil erosion grades (Slight, Light, Moderate, Intense, Extremely Intense, and Severe Erosion) instead of actual erosion rates. Table S11 summarizes areas corresponding to different erosion grades in the 31 provinces in China, derived from reports released by the Ministry of Water Resources, PR China (29). Table S3 lists the conversion rules from erosion grades to erosion rates. Note that each specific erosion grade corresponds to a range of erosion rates, v_{ero} is determined as the medium value within the range. The uncertainty induced by such simplification has been included by presenting the error bars of the relevant estimates (see Table S1). Section 3 also examines the sensitivity of v_{ero}.

2.2 Vertical distribution of soil organic carbon

The soil organic carbon content of 8 vertical layers (i.e. 0–0.045, 0.045–0.091, 0.091–0.166, 0.166–0.289, 0.289–0.493, 0.493–0.829, 0.829–1.383 and 1.383–2.296 m) for each of 8980 soil profiles was obtained from a Global Soil Dataset based on the Soil Map of the World and various regional and national soil databases (http://globalchange.bnu.edu.cn/research/soil2). The soil-type-and-polygon-linkage method was used to derive the spatial distribution of soil properties (30), in which data describing soil properties were interpolated from natural soil horizons to standard layers using equal-area quadratic smoothing spline functions. This has previously been proved to be of advantage in predicting the depth function of soil properties (30). The smoothing parameter of the spline was set as 0.1. The spline was used to estimate parameters for various soil properties in the standard layers, while negative values were set to zero. The resolution was 30 arc-seconds (about 1 km at the equator). The dataset was then used to derive parameters describing the vertical profile of SOC, namely $C_{SOC\text{-}top}$, C_{min}/C_0 and k, following the process presented in Fig. S2.

2.3 Carbon pool turnover rates and net primary production

The turnover rate of the carbon pool refers to the ratio of soil respiration to total carbon storage (k_O in equations (13) and (14)). Net primary production (NPP) is regarded as the total input of carbon from vegetation to the soil carbon pool (I_B in equations (13) and (14)). These two parameters are extracted from the outputs of ten state-of-the-art global carbon cycle models, namely CLM4C (31, 32), CLM4CN (31, 32), HYLAND-v4 (33), LPJ (34), LPJ_GUESS (35), ORCHIDEE (36), SDGVM (37,

38), TRIFFID (41), VEGAS-2.1 (42), OCN (43), and averaged over the period from 1980s to present. Mean values and variances of NPP and k_O derived from the ten models are presented in Table S12.

2.4 Precipitation

Precipitation data (Fig. S6(b)) were collected from the website of China Meteorological Administration (http://www.cma.gov.cn/2011qxfw/2011qsjgx/). 675 stations were included and the data series covered from 1995 to 2012 (Fig. S7).

2.5 Vegetation cover

Data on vegetation cover were extracted from the 1:1,000,000 map of China's Vegetation Cover published in 2007. This dataset is regarded as an integrated outcome based on long-term observations, which could reflect the general condition of vegetation cover distribution from 1980s to 1990s (Fig. S6(c)). Herein, vegetation type was not directly used for calculation of carbon fluxes; instead its influence has been implicitly accounted in the final C budget estimation via soil erosion rate.

2.6 Parameters derived from the national-scale datasets

Table S13 summarizes the parameters used to calculate the five fluxes in the datasets presented above.

3. Uncertainty and sensitivity analysis

3.1 Dynamic replacement in the erosional area

This approach assumes that all NPP enters into the soil carbon pool, and adopts a k_O coefficient that includes the effect of initial rapid carbon decomposition. In the present uncertainty analysis, this assumption is tested by assuming a humification coefficient of 30% (as in an agricultural ecosystem) and 10% (as in grassland and forest ecosystems). Correspondingly, 30% and 10% of the k_O dataset is adopted, because the lower carbon input requires a lower carbon turnover rate to reach equilibrium (see Section 2.1 in the Supporting Material in Van Oost et al. (2) which showed that k_O changes proportionally with I_B when the carbon pool is in a balanced state). The results show that F3 reduced by 7.5% and 13.7% when I_B decreased by 70% and 90%. The variation in the estimate of NPP also reflects the uncertainty induced by different levels of carbon input. Here, values for NPP were extracted from the CLM4C, CLM4CN, HYLAND-v4, LPJ, LPJ_GUESS, ORCHIDEE, SDGVM, TRIFFID, VEGAS-2.1 and OCN models, and the erosion-induced CO_2 fluxes in China calculated accordingly. Table S12 shows that inputs from the ORVHIDEE model with the largest mean NPP (0.42 kg/m^2/yr) produced the largest total carbon sequestration of 64.6 Mt C/yr based on the erosion data from the 2nd National Survey in 1995–1996 and 53.2 Mt C/yr based on the erosion data from the

4^{th} National Survey in 2010–2012. However, parameters derived from the CLM4C model with the lowest mean NPP (0.30 $kg/m^2/yr$) generated the lowest CO_2 absorption of 28.1 Mt C/yr and 29.2 Mt C/yr based on the two national surveys in 1995–1996 and 2010–2012, respectively. The SDGVM, HYLAND-v4 and LPJ_GUESS models with NPP close to the average level of the ten models gave results that most closely fitted the average values of CO_2 absorption, with errors less than 5%. Parameters from SDGVM and HYLAND-v4 models led to best fits, whereas those from CLM4C, ORCHIDEE, VEGAS-2.1 and OCN models produced results with errors > 20%. It should be noted that as SOC declines due to continuous erosion, k_O from these models could be over-estimated (8). However, since the mean k_O of each model changes within a narrow range (0.02–0.04 yr^{-1}), k_O should contribute little to the variation of the outputs of the ten models.

A sensitivity analysis has been carried out to examine the uncertainty induced by NPP. The results indicate that NPP is positively correlated to CO_2 flux; when NPP is altered by 20%, the relative change in CO_2 sink intensity is about 29%. Similarly, the erosion rate is also positively related to CO_2 flux, and a 20% change in erosion rate would lead to a 23% change in CO_2 sink intensity. However, the carbon turnover rate and carbon content in the surface layers are negatively correlated, and less sensitive. A 20% change in carbon turnover rate and surface soil carbon content leads to 13% and 9% changes in CO_2 sink intensity, respectively.

Another source of uncertainty is introduced by the assumption that erosion does not influence the rate of SOC decomposition, which is problematic at the timescale of decades; instead, a conceptual model should link k_O and k_E. However, little quantitative information is yet available to develop such a model. Furthermore, studies have shown that accurate predictions of both SOC density profiles and SOC quality can be obtained from simulations where k_O is assumed to be independent of k_E (see Wang et al., (42), Nadeu et al., (43), Lugato et al., (44)). We therefore suggest that the assumption of independence is reasonable, particularly for a large-scale modelling assessment.

As another source of vertical loss, DOC leaching from topsoil has been ignored in the present approach. As suggested by Li et al. (45), Long et al. (46), and Gou et al. (47), the DOC leaching potential ranges from 3.8–8.7 kg/ha (in other words, 0.55–0.96 Mt C/yr). Based an empirical formula previously developed for hillslope croplands in China, which assumed that DOC leaching depends directly on precipitation, the DOC leaching potential throughout China has also been estimated to be 0.94 Mt C/yr, using the yearly averaged precipitation data from 1995 to 2012. The foregoing results indicate that the potential DOC leaching flux in China is negligible compared with F3.

3.2 Carbon content in the surficial layer

The carbon content in the surficial layer is regarded as constant (obtained from the surficial 4.5 cm layer of soil obtained from the national survey) to calculate F1, F2, and F4. In areas of the Erosion Grade 2 or 3 (erosion rate = 0.74–1.90 mm/yr, 1.90–3.70 mm/yr, respectively) which cover the majority of the surface area of China, the 4.5 cm surficial layer has not been eroded during the period of interest, and it is reasonable to assume that the top layer carbon content remains constant. However, in areas where erosion rate larger than 0.37 mm/a, F1, F2, and F4 could possibly be overestimated, consequently leading to a relatively lower VLC ratio. This implies that the lateral carbon fluxes could be lower, and the ability of recovering lost carbon could be even higher in North China (inclusive of the Loess Plateau) and Southwest China (in the Upper Yangtze) (48).

References

1. Jing K, Wang WZ, Zheng FL (2005) *Soil Erosion and Environment in China* (Science Press, Beijing). (in Chinese)
2. Van Oost K, et al. (2007) The impact of agricultural soil erosion on the global carbon cycle. *Science* 318: 626–629.
3. Schmidt MWI, et al. (2011) Persistence of soil organic matter as an ecosystem property. *Nature* 478(7367): 49–56.
4. Berhe AA, Kleber M (2013) Erosion, deposition, and the persistence of soil organic matter: mechanistic considerations and problems with terminology. *Earth Surf Process Landf* 38: 908–912.
5. Chappell A, Rossel RAV, Loughran R (2011) Spatial uncertainty of Cs-137-derived net (1950s-1990) soil redistribution for Australia. *J Geophys Res*

Atmosph 116(F4): F4015–F4036.

6. Chappell A, Webb NP, Rossel RAV, Bui E (2014) Australian net (1950s-1990) soil organic carbon erosion: implications for CO_2 emission and land-atmosphere modeling. *Biogeosciences* 11(18): 5235–5244.
7. Berhe AA, Harden JW, Torn MS, Harte J (2008) Linking soil organic matter dynamics and erosion-induced terrestrial carbon sequestration at different landform positions. *J Geophys Res* 113(G4): 4647–4664.
8. Chappell A, Baldock J, Sanderman J (2016) The global significance of omitting soil erosion from soil organic carbon cycling schemes. *Nat Clim Change* 6: 184–191.
9. Xu Y, Yang B, Liu GB, Liu PL (2009) Topographic differentiation simulation of crop yield and soil and water loss on the Loess Plateau. *J Geogr Sci* 19: 331–339.
10. Su ZA, Zhang JH, Nie XJ (2010) Effect of soil erosion on soil properties and crop yields on slopes in the Sichuan Basin, China. *Pedosphere* 20: 736–746.
11. Ni JR, Li XX, Borthwick AGL (2008) Soil erosion assessment based on minimum polygons in the Yellow River basin, China. *Geomorphology* 93: 233–252.
12. Ni JR, Wu A, Li TH, Yue Y, Borthwick AGL (2014) Efficient soil loss assessment for large basins using smart coded polygons. *J Environ Inform* 23: 47–57.
13. Fang HY, Li QY, Sun LY, Cai QG (2012) Using ^{137}Cs to study spatial patterns of soil erosion and soil organic carbon (SOC) in an agricultural catchment of the typical black soil region, Northeast China. *J Environ Radioactiv* 112: 125–132.

14. Liang AZ, et al. (2009) Estimation of total erosion in cultivated Black soils in northeast China from vertical profiles of soil organic carbon. *Eur J Soil Sci* 60: 223–229.

15. Zhang JH, Ni SJ, Su ZA (2012) Dual roles of tillage erosion in lateral SOC movement in the landscape. *Eur J Soil Sci* 63: 165–176.

16. Zhang JH, Li FC (2013) Soil redistribution and organic carbon accumulation under long-term (29 years) upslope tillage systems. *Soil Use Manage* 29: 365–373.

17. Tang XY, Yang H, Du MY, Zhao QG, Li RY (2003) Soil redistribution investigations by combined use of soil ^{137}Cs and selected chemical properties. *Soil Sci Plant Nutr* 49: 557–566.

18. Liu S, Bliss N, Sundquist E, Huntington TG (2003) Modeling carbon dynamics in vegetation and soil under the impact of soil erosion and deposition. *Global Biogeochem Cy* 17: 1074–1097.

19. Van Oost K, et al. (2005) Landscape-scale modeling of carbon cycling under the impact of soil redistribution: The role of tillage erosion. *Global Biogeochem Cy* 19: GB4014.

20. Van Oost K, et al. (2012) Legacy of human-induced c erosion and burial on soil-atmosphere C exchange. *Proc Natl Acad Sci* 109(47): 19492–19497.

21. Wang Z, et al. (2014) The fate of buried organic carbon in colluvial soils: a long-term perspective. *Biogeosciences* 11(3): 873–883.

22. Jacinthe PA, Lal R, Kimble JM (2001) Organic carbon storage and dynamics in

croplands and terrestrial deposits as influenced by subsurface tile drainage. *Soil Sci* 166(5): 322–335.

23. Guenet B, et al. (2014) Fast mineralization of land-born C in inland waters: first experimental evidences of aquatic priming effect. *Hydrobiologia* 721: 35–44.

24. Van Hemelryck H, Govers G, Van Oost K, Merckx R (2010) The effect of soil redistribution on soil organic carbon: an experimental study. *Biogeosciences* 7(12): 3971–3986.

25. Ministry of Water Resources, PRC, China Water & Power Press, Beijing (1997) *Criterion of Classification of Soil Erosion*. (in Chinese)

26. Liu BY, Zhang KL, Xie Y (2001) An empirical soil loss equation. *Proceedings of 12th ISCO* (Tsinghua Univ. Press, Beijing), pp. 143–149.

27. Du HQ, Xue X, Wang T (2015) Mapping the risk of water erosion in the watershed of the Ningxia-Inner Mongolia Reach of the Yellow River, China. *J Mt Sci-Engl* 12(1): 70–84.

28. Miao CY, Ni JR, Borthwick AGL, Yang L (2011) A preliminary estimate of human and natural contributions to the changes in water discharge and sediment load in the Yellow River. *Global Planet Change* 76(3–4): 196–205.

29. Ministry of Water Resources, PRC, National Bureau of Statistics, PRC, (2013) *Bulletin of First National Census for Water* (China Water & Power Press, Beijing). (in Chinese)

30. Shang Guan W, Dai YJ, Liu BY, Ye AZ, Yuan H (2012) A soil particle-size distribution dataset for regional land and climate modelling in China. *Geoderma*

171–172: 85–91.

31. Oleson KW, et al. (2010) *Technical description of version 4.0 of the Community Land Model (CLM)*. (NCAR Technical Note, National Center for Atmospheric Research, Boulder, Colorado, USA).

32. Lawrence DM, et al. (2001) Parameterization improvements and functional and structural advances in Version 4 of the Community Land Model. *J Adv Model Earth Syst* 3: M03001.

33. Levy PE, Cannell MGR, Friend AD (2004) Modelling the impact of future changes in climate, CO_2 concentration and land use on natural ecosystems and the terrestrial carbon sink. *Global Environ Chang* 14: 21–30.

34. Sitch S, et al. (2003) Evaluation of ecosystem dynamics, plant geography and terrestrial carbon cycling in the LPJ dynamic global vegetation model. *Global Change Biol* 9: 161–185.

35. Smith B, Prentice IC, Sykes MT (2001) Representation of vegetation dynamics in the modelling of terrestrial ecosystems: comparing two contrasting approaches within European climate space. *Global Ecol Biogeogr* 10: 621–637.

36. Krinner G, et al. (2005) A dynamic global vegetation model for studies of the coupled atmosphere-biosphere system. *Global Biogeochem Cy* 19: GB1015.

37. Woodward FI, Smith TM, Emanuel WR (1995) A global land primary productivity and phytogeography model. *Global Biogeochem Cy* 9: 471–490.

38. Woodward FI, Lomas MR (2004) Simulating vegetation processes along the Kalahari transect. *Global Change Biol* 10: 383–392.

39. Cox PM (2001) *Description of the "TRIFFID" dynamic global vegetation model*. (Technical Note 24, Hadley Centre, Met Office, Bracknell, Berks U.K.).

40. Zeng N, Qian H, Roedenbeck C, Heimann M (2005) Impact of 1998–2002 midlatitude drought and warming on terrestrial ecosystem and the global carbon cycle. *Geophys Res Lett* 32: L22709.

41. Zaehle S, Friend AD (2010) Carbon and nitrogen cycle dynamics in the O-CN land surface model: 1. Model description, site-scale evaluation, and sensitivity to parameter estimates. *Global Biogeochem Cy* 24: GB1005.

42. Wang Z, Doetterl S, Vanclooster M, Van Wesemael B, Van Oost K (2015) Constraining a coupled erosion and soil organic carbon model using hillslope-scale patterns of carbon stocks and pool composition. *J Geophys Res Biogeosci* 120: 452–465.

43. Nadeu E, Gobin A, Fiener P, Van Wesemael B, Van Oost K (2015) Modelling the impact of agricultural management on soil carbon stocks at the regional scale: the role of lateral fluxes. *Global Change Biol* 21(8): 3181–3192.

44. Lugato E, Paustian K, Panagos P, Jones A, Borrelli P (2016) Quantifying the erosion effect on current carbon budget of European agricultural soils at high spatial resolution Erosion integration in the European C balance. *Global Change Biol*. DOI: 10.1111/gcb.13198. First published: 23 February 2016.

45. Li TK, Zhu B, Wang XG, Kou CL (2013) Characteristics of dissolved organic carbon leaching from hillslope cropland of purple soil in the Sichuan Basin, China. *J Food Agric Environ* 11(2):1522–1527.

46. Long GQ, Jiang YJ, Sun B (2015) Seasonal and inter-annual variation of leaching of dissolved organic carbon and nitrogen under long-term manure application in an acidic clay soil in subtropical China. *Soil Tillage Res* 146: 270–278.
47. Gou XL, et al. (2013) Effect of Changes in Seasonal Freeze-thaw Pattern on DOC Loss from Leaching in the Alpine Forest Soil. *Journal of Soil and Water Conservation* 27(6): 205–210. (in Chinese)
48. Li Y, et al. (2015) Sustained high magnitude erosional forcing generates an organic carbon sink: test and implications in the Loess Plateau, China. *Earth Planet Sci Lett* 411: 281–289.
49. Wang X, Ma H, Li R, Song Z, Wu J (2012) Seasonal fluxes and source variation of organic carbon transported by two major Chinese Rivers: The Yellow River and Changjiang (Yangtze) River. *Global Biogeochem Cy* 26(2): GB2025.
50. Wang L, Song C, Guo Y (2015) The spatiotemporal distribution of dissolved carbon in the main stems and their tributaries along the lower reaches of Heilongjiang River Basin, Northeast China. *Environ Sci Pollut R*: 1–14.
51. Zhu X, Yu G, Gao Y, Wang Q (2012) Fluxes of particulate carbon from rivers to the ocean and their changing tendency in China. *Progress in Geography* 31(1): 118–122. (in Chinese)
52. Ni H, Lu F, Luo X, Tian H, Zeng E (2008) Riverine inputs of total organic carbon and suspended particulate matter from the Pearl River Delta to the coastal ocean off South China. *Mar Pollut Bull* 56(6): 1150–1157.
53. Zhang LK, Qin XQ, Yang H, Huang QB, LiuPY (2013) Transported fluxes of the

riverine carbon and seasonal variation in pearl river basin. *Chinese Journal of Environmental Science* 34(8): 3025–3034. (in Chinese)

54. Xia B, Zhang L (2011) Carbon distribution and fluxes of 16 rivers discharging into the Bohai Sea in summer. *Acta Oceanol Sin* 30(3): 43–54.
55. Xu JX, Sun J (2004) Effect of erosion control measures on sediment delivery ratio. *Advances in Water Science* 15(1): 29–34. (in Chinese)
56. Gong SZ, Xiong SG (1979) Sources and regional distribution of sediments in the Yellow River. Yellow River 1(1): 7–17.
57. Cai QG, Chen H, Ma SJ (1991) Sediment Delivery Ratio of a single storm in the Yangdaogou watershed in the hilly loess region. *Proceedings of Environmental Evolution and the Regularities of Water and Sediment Movement in the Yellow River Basin* (Geology Press, Beijing). (in Chinese)
58. Jing K (1999) Studies on the sediment delivery in the Jinghe and Beiluohe Basins. *Yellow River* 21(12):18–19. (in Chinese)
59. Mu JZ, Meng QM (1982) Sediment Delivery Ratio in the calculation of sediment yield in river basins. *Journal of Sediment Research* 2: 60–65. (in Chinese)
60. Cao H, et al. (2001) Primary estimate on soil loss amounts in Yangtse Delta Region using ^{137}Cs technique. *Journal of Soil and Water Conservation* 15(1): 13–15. (in Chinese)
61. Yu JR, Shi LR, Feng MH, Li RH (1991) The surface erosion and fluvial silt in the upper reaches of Changjiang river. *Bulletin of Soil and Water Conservation* 11(1): 9–17. (in Chinese)

62. Zhang FZ (1993) On Sediment Delivery Ratio. *Science of Soil and Water Conservation* 10: 17–18. (in Chinese)

63. Wei ZG (2004) Second stage of the key conservation project to the upper Yongding River Basin, Datong City. *Science of Soil and Water Conservation* Suppl. Issue: 26–27. (in Chinese)

64. Wu CJ, Gan ZM (1998) The problem about the river silt delivery ratio in South Shaanxi. *Scientia Geographica Sinica* 18(1): 39–44.

65. Ma K, Wang ZQ, Chen X, Sui GP, Yang SP (2003) Study of erosion on the neutron activate analysis of the fixed soil core eu tracer on red soil slope. *Journal of Zhejiang University* 29(4): 361–367. (in Chinese)

66. Liu Y, Zhang P (1995) Surface erosion in upper Yangtze Region and river sediment transport. *Journal of Yangtze River Scientific Research Institute* 12(1): 40–44. (in Chinese)

67. Li ZG, Liu BZ (2006) Calculation on soil erosion amount of main river basin in China. *Science of Soil and Water Conservation* 4(2): 1–6. (in Chinese)

68. Fan JR, Zhong XH, Liu SZ (2003) Remote-sensing-based monitoring on soil erosion and sediment delivery in typical watersheds in the middle and lower regions of the Jianglingjiang River Basin. *Science in China Series E* 33(S1): 157–163. (in Chinese)

69. Zeng QM, et al. (1996) Remote sensing investigation and analysis of water and soil loss in the upper reaches of Miyun Reservoir. Journal of Soil and Water Conservation 2(1): 46–49. (in Chinese)

70. Lu J (1989) Preliminary study on variation of erosion and sediment yield of drainage basins in Yanshan, north China, associated with geology and geomorphology. *Journal of Sediment Research* 1: 25–83. (in Chinese)

71. Niu XY (2015) Soil Erosion and Nutrient Variability Under LUCC in the Small Catchment of Dianchi. (Doctoral dissertation, Nanjing Normal University). (in Chinese)

72. Chen DL (2004) Studies on the Effects and Mechanism of Soil and Water Conservation under Different Forest Restoration Types in Sloping Field of Red Soil Region. (Doctoral dissertation, Hunan Agricultural University). (in Chinese)

73. Deng RF, Wang BQ, Liu PL, Liu D, Jia XU (2011) Effects of different land use patterns on soil organic carbon loss on the loess slope. *Research of Soil and Water Conservation* 15(5): 104–107. (in Chinese)

74. Jia SW (2010) Soil Organic Carbon Loss through Water Erosion in Loess Hilly Region of Northwestern China. *4th International Conference on Management and Service Science, IEEE* (Wuhan, China), pp. 1–4.

75. Wang BQ (2004) The Dynamics and Transfer of Soil Organic Carbon and Nitrogen in the Scenario of Erosion and Aridity in the Loessial Region. (Doctoral dissertation, Northwest A&F University). (in Chinese)

76. Ma W, et al. (2014) Effect of soil erosion on dissolved organic carbon redistribution in subtropical red soil under rainfall simulation. *Geomorphology* 226(226): 217–225.

77. Jiang QL, Xie YS, Zhang YL, Zhang H, Hao XD (2011) Soil erosion in a small

watershed in water source areas of Beijing and Tianjin: Spatial simulation. *Chinese Journal of Ecology* 30(8): 1703–1711. (in Chinese)

78. Qin W, Zuo CQ, Zheng HJ, Ma L, Du PF (2013) Determination of key factors of soil loss equation of red-soil sloping land in northern Jiangxi Province. *Transactions of the Chinese Society of Agricultural Engineering* 29(21): 115–125. (in Chinese)

79. Jiao J (2010) Study on Spatial Variation of Soil Erosion in Northeastern China. *Research of Soil and Water Conservation* 17(3): 1–6. (in Chinese)

80. Ju ZS et al. (2015) Evaluation of soil erosion in small watershed of the Three Gorges Reservoir Region by Using ^{137}Cs, ^{210}Pb and CSLE. *Journal of Soil and Water Conservation* 29(3): 75–80. (in Chinese)

81. Yang SY (2014) The analysis of soil erosion pattern in National key harnessing areas of Yimeng Mountains based on CSLE models. (Doctoral dissertation, Shandong Agricultural University). (in Chinese)

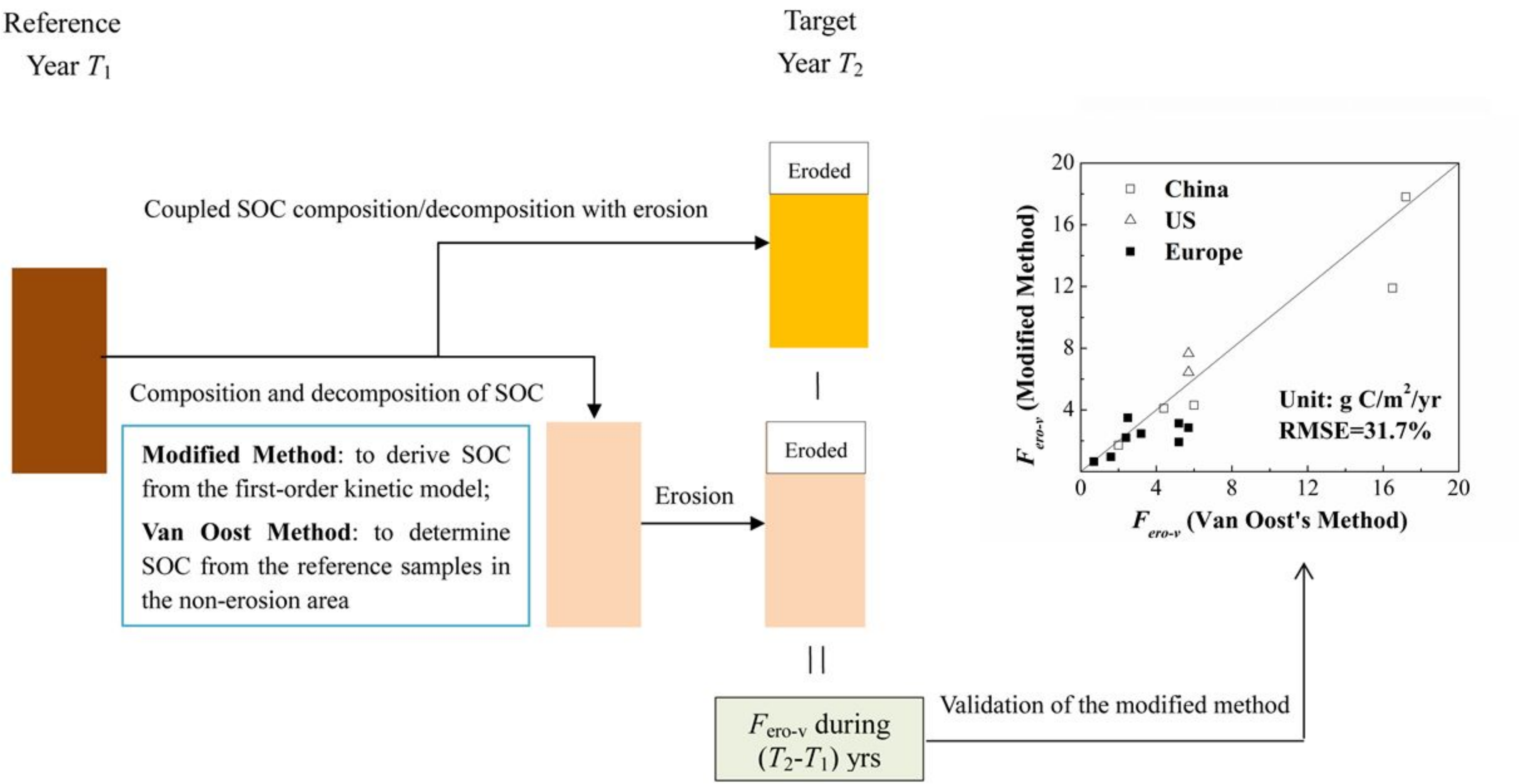

Fig. S1. Comparison between Van Oost et al.'s (2) and modified methods based on data from small watersheds in China and Europe.

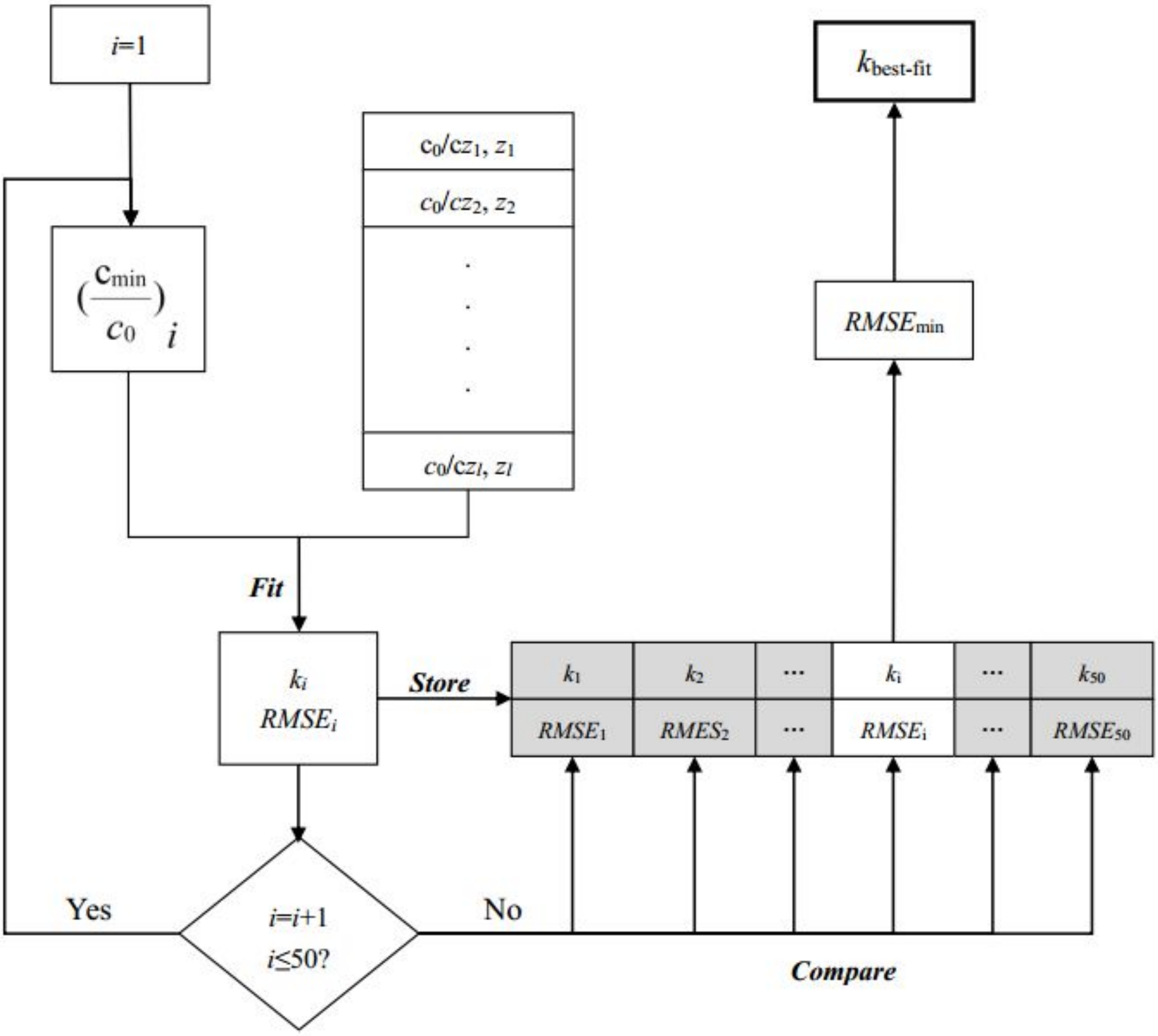

Fig. S2. Flow chart showing how the initial SOC profile is determined.

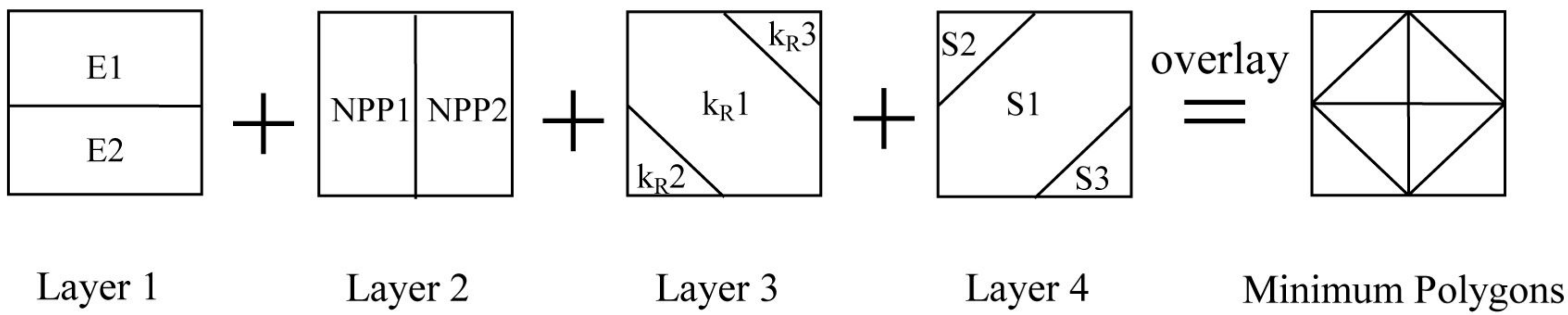

Fig. S3. Generation of the minimum polygon.

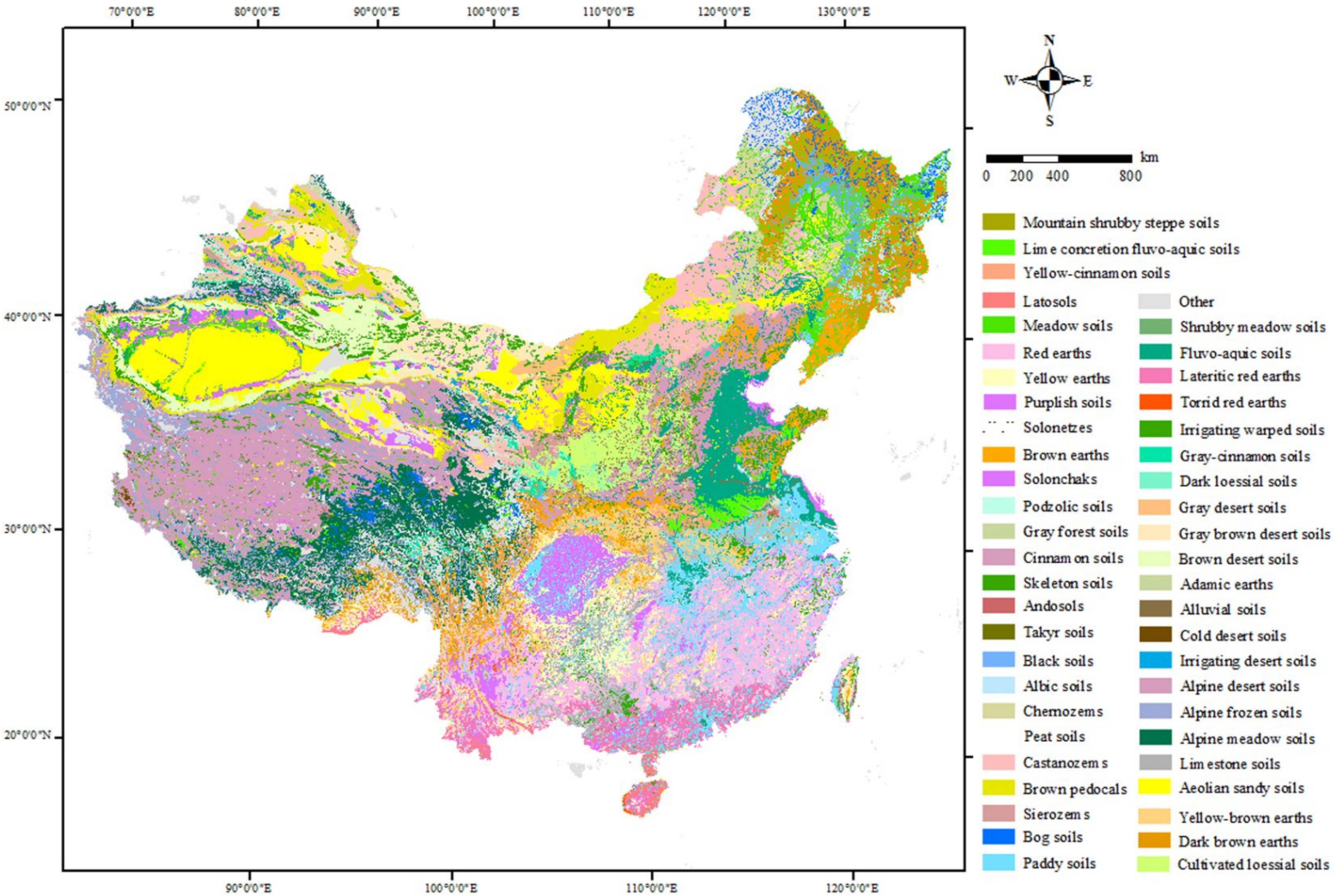

Fig. S4. Spatial distribution of different soil types in China, produced using ArcGIS 10.0 software.

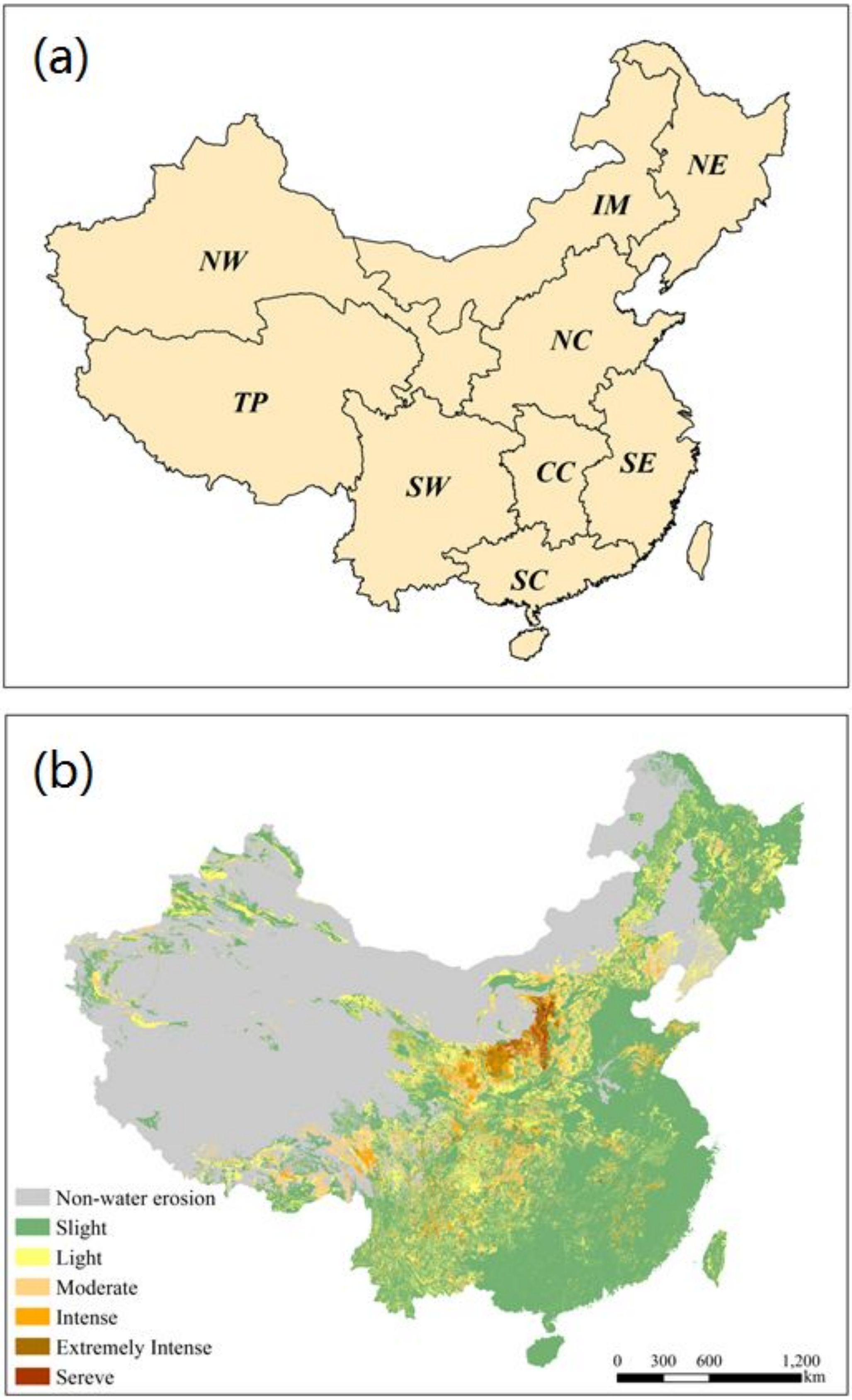

Fig. S5. (a) Nine sub-regions in China and (b) Zonation map for water erosion grades in China based on data from National Survey of Soil Erosion in 1995–1996 (CC: Central China; IM: Inner Mongolia; NC: North China; NE: Northeast China; NW: Northwest China; SC: South China; SE: Southeast China; SW: Southwest China; TP: Tibet Plateau)

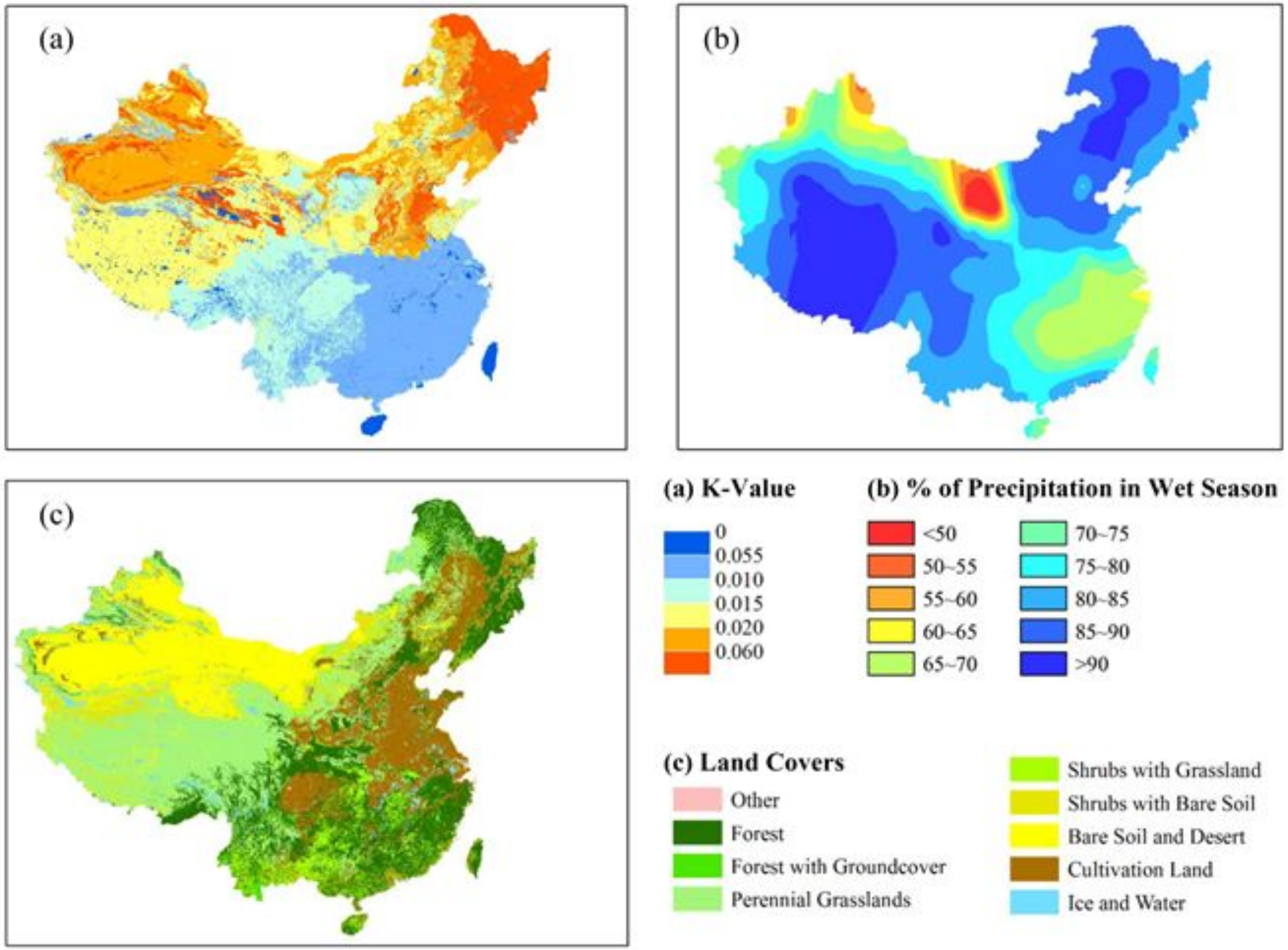

Fig. S6. Distribution of (a) K-value as an indicator of soil erodibility; (b) percentage of precipitation in wet season in China (from April to September); and (c) agricultural land.

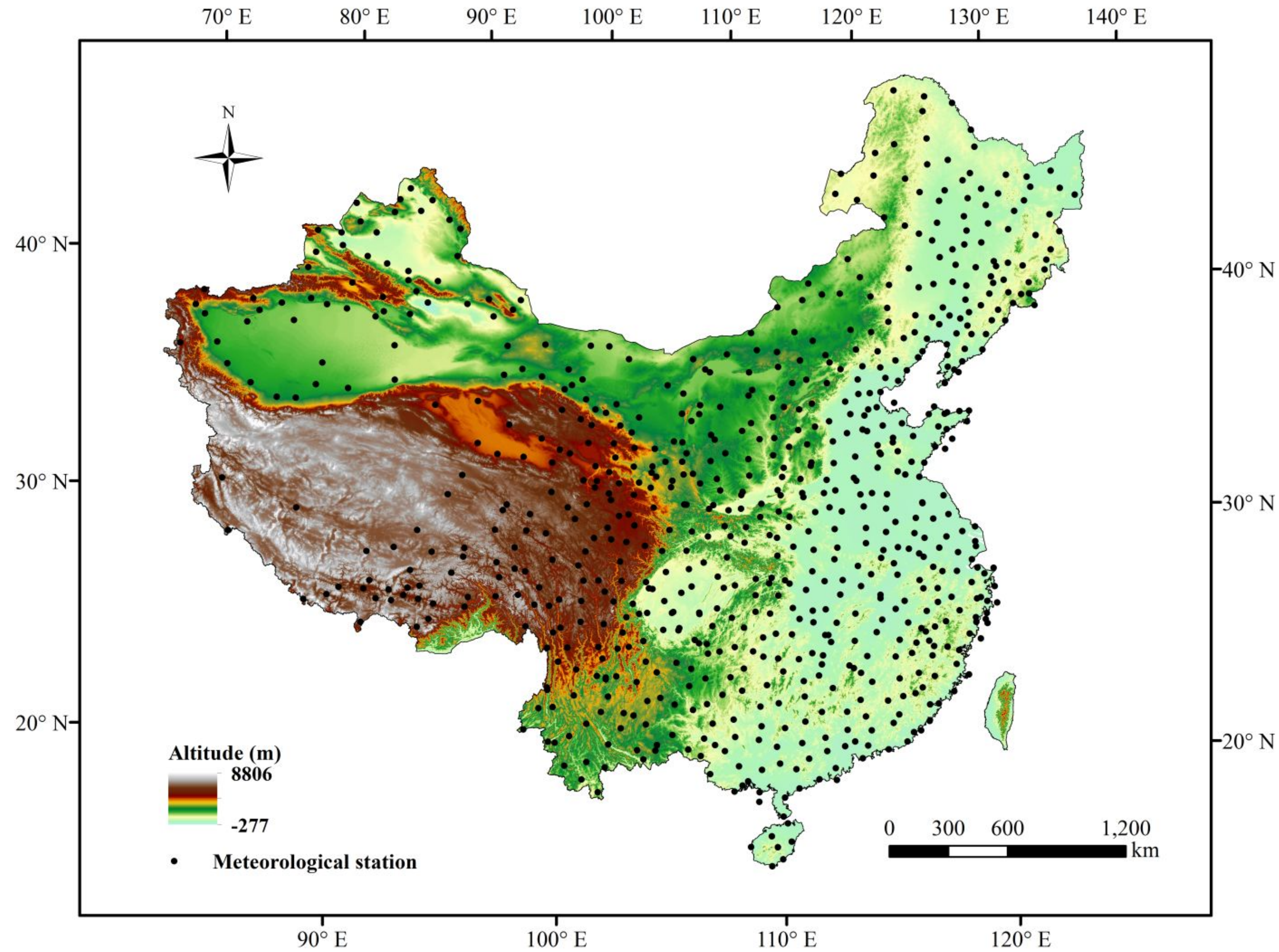

Fig. S7. Locations of the 675 Meteorology Stations in China.

Table S1. Regional distribution of the five flux components for each sub-region

Region	Total Area M km²	Erosional Area 10^6 km²		F1 Mt C/yr		F2 Mt C/yr		F3 Mt C/yr		F4 Mt C/yr		F5 Mt C/yr		F1-F2 Mt C/yr		F3 – (F4+F5) Mt C/yr	
		1[a]	2[b]	1[a]	2[b]	1[a]	2[b]	1[a]	2[b]	1[a]	2[b]	1[a]	2[b]	1[a]	2[b]	1[a]	2[b]
CC	9.50	0.08	0.07	9.70 ±4.30	6.00 ±2.70	5.80 ±3.40	4.20 ±2.50	3.84 ±1.26	2.85 ±1.38	0.12 ±0.07	0.08 ±0.04	0.14 ±0.08	0.07 ±0.04	3.90 ±2.30	1.90 ±1.10	3.59 ±1.40	2.70 ±1.46
IM	1.14	0.15	0.10	12.80 ±5.70	5.40 ±2.40	7.70 ±4.60	4.20 ±2.50	1.90 ±1.28	1.03 ±0.61	0.04 ±0.02	0.04 ±0.02	0.03 ±0.02	0.03 ±0.02	5.10 ±30	1.20 ±0.70	1.83 ±1.32	0.96 ±0.65
NC	0.90	0.30	0.21	25.50 ±11.30	12.50 ±5.60	8.70 ±5.20	7.40 ±4.40	12.80 ±9.03	6.10 ±4.25	0.07 ±0.04	0.05 ±0.03	0.11 ±0.07	0.05 ±0.03	16.80 ±9.90	5.10 ±3.00	12.62 ±9.14	6.00 ±4.31
NE	0.79	0.15	0.15	19.90 ±8.80	21.50 ±9.60	14.00 ±8.30	13.40 ±7.90	3.59 ±1.89	6.10 ±2.94	0.12 ±0.07	0.11 ±0.06	0.11 ±0.06	0.12 ±0.07	5.90 ±3.50	8.10 ±4.80	3.37 ±2.02	5.87 ±3.07
NW	2.10	0.28	0.17	26.70 ±11.90	13.80 ±6.20	12.80 ±7.60	9.10 ±5.40	3.91 ±3.58	1.39 ±1.36	0.02 ±0.01	0.02 ±0.01	0.03 ±0.02	0.01 ±0.01	13.90 ±8.20	4.70 ±2.80	3.86 ±3.61	1.36 ±1.38
SC	0.45	0.01	0.08	0.70 ±0.30	6.00 ±2.70	0.60 ±0.30	4.70 ±2.80	1.20 ±1.14	2.20 ±1.73	0.10 ±0.05	0.10 ±0.06	0.09 ±0.05	0.11 ±0.07	0.20 ±0.10	1.30 ±0.80	1.02 ±1.25	1.98 ±1.86
SE	0.68	0.07	0.07	6.40 ±2.90	4.40 ±2.00	4.60 ±2.80	4.10 ±2.40	4.69 ±2.53	3.41 ±1.85	0.17 ±0.09	0.10 ±0.06	0.25 ±0.15	0.09 ±0.05	1.80 ±1.10	0.40 ±0.20	4.27 ±2.78	3.22 ±1.95
SW	1.13	0.46	0.31	67.00 ±29.80	40.50 ±18.00	33.70 ±20.00	18.40 ±10.90	17.91 ±5.02	17.30 ±5.54	0.28 ±0.15	0.23 ±0.13	0.32 ±0.19	0.26 ±0.16	33.30 ±19.70	22.10 ±13.10	17.31 ±5.37	16.81 ±5.82
TP	1.92	0.11	0.10	57.50 ±25.60	23.00 ±10.20	24.60 ±14.60	17.50 ±10.40	2.21 ±2.10	1.56 ±1.52	0.10 ±0.05	0.06 ±0.04	0.12 ±0.07	0.06 ±0.03	32.90 ±19.50	5.50 ±3.20	2.00 ±2.23	1.44 ±1.59
SUM	9.50	1.61	1.26	226.30 ±100.70	133.20 ±59.30	112.50 ±66.80	82.90 ±49.20	52.05 ±27.84	41.94 ±21.17	1.00 ±0.56	0.80 ±0.44	1.20 ±0.72	0.80 ±0.48	113.80 ±67.30	50.30 ±29.80	49.85 ±29.11	40.34 ±22.09
Average		1.44		179.80±80.00		97.70±58.00		47.00±24.50		0.90±0.50		1.00±0.60		82.00±48.60		45.10±25.60	

a: based on the erosion data from the 2nd National Survey in 1995–1996

b: based on the erosion data from the 4th National Survey in 2010–2012.

Table S2. POC and DOC fluxes of seven major rivers in China

Basin	Drainage Area (km^2)	Sediment Delivery Mt/yr	POC Flux (Tg/yr)	DOC Flux (Tg/yr)	Observation Year(s)	Reference
Yangtze River	1,705,383	407.9	1.520	1.580	2009	(49)
Yellow River	752,032	766.6	0.389	0.032	2009	(49)
Helongjiang	-	-	-	1.570	2009–2010	(50)
Songhua Jiang	528,300	407.9	0.266	-	2003–2009	(51)
Pearl Delta	-	-	0.500	0.400	2005–2006	(52)
Pearl River	415,200	766.6	2.500	1.130	2012	(53)
Liao River	120,764	11.1	0.048	0.022	2005	(54)
Hai River	95,971	8.0	0.038	0.038	2005	(54)
Huai River	131,600	10.5	0.150	-	2003–2009	(51)

Table S3. Conversion from erosion grade to erosion rate, with corresponding *SDR* range (1, 25).

Erosion Grade	Erosion Modulus ($t \cdot km^{-2} \cdot a^{-1}$)	Erosion Rate ($mm \cdot a^{-1}$)	*SDR* Grade
1 (Slight)	< 200, 500, 1000	< 0.15, 0.37, 0.74	-
2 (Light)	200, 500, 1000–2500	0.15, 0.37, 0.74–1.90	0.1–0.3
3 (Moderate)	2500–5000	1.90–3.70	0.3–0.5
4 (Intense)	5000–8000	3.70–5.90	0.5–0.7
5 (Extremely Intense)	8000–15000	5.90–11.10	0.7–0.9
6 (Severe)	> 15000	> 11.10	0.9–1.0

Table S4. Summary of values of available *SDR* in representative areas throughout China

Site	Region	Erosion Grade	*SDR*	Reference
Wuding Basin	North China	VI	1.00	(55)
Loess Plateau	North China	VI	1.00	(56)
Yangdaogou	North China	VI	1.00	(57)
Liujia Basin	North China	VI	0.91	(58)
Dali Basin	North China	V	0.80–1.31	(59)
Middle Yellow River	North China	IV	0.70–1.00	(60)
West Han Basin	South China	IV	0.66	(61)
Pearl Basin	South China	III	0.36–0.41	(62)
Han Basin	South China	II	0.27–0.55	(62)
Yongding Basin	North China	II	0.26	(63)
Hainan Province	South China	II	0.26–0.62	(62)
Shannxi Province	Northwest	II	0.24–0.59	(64)
Lanxi Basin	South China	II	0.20–0.35	(65)
Jiangling Basin	Southwest	II	0.14–0.61	(66)
Songhuajiang Basin	Northeast	II	0.12	(67)
Lizi Basin	Southwest	II	0.11–0.27	(68)
Chaobai Basin	North China	II	0.10–0.26	(69)
Yan Mountain	North China	II	0.15–0.69	(70)

Table S5. Comparison of F1 and F2 components with data on SOC removal and deposition collected from small watersheds in different regions throughout China.

Reference	Region	Location	Published SOC removal	F1 in this paper	Published SOC deposition	F2 in this paper
			kg/km²/yr		kg/km²/yr	
(71)	SW	102°34’E, 25°6’ N	21,330	11,112–45,221	-	-
(72)	CC	27°05’N, 112°18’E	33,150	20,244–46,058	-	-
(73)	NC	109°27’E, 36°26′N	16,320	10,271–24,080	-	-
(74)	NC	36°58′N, 109°11′E	8,942	6,629–14,513	-	-
(13)	NE	125°16′E, 48°42′N	42,600	12,811–67,533	-	-
(75)	NC	109°13′E, 36°42′N	-	-	14,690	9,690–22,717
(13)	NE	125°16′E, 48°42′N	-	-	32,500	8,585–58,762
(76)	NE	44.7°N, 125.9°E	-	-	18,994	13,505–52,014

Table S6. Crop yields of 31 provinces in the 1990s and 2010s (i.e.: 2010–2015)*

Province	1990s			2010s		
	Cropland Area (10^3 ha)	Crop Yield (10^3 t)	Crop Yield/Area (kg/ha)	Cropland Area (10^3 ha)	Crop Yield (10^3 t)	Crop Yield/Area (kg/ha)
Beijing	427	2,374	5,560	194	1,138	5,871
Tianjin	451	2,070	4,585	323	1,618	5,009
Hebei	7,137	27,895	3,909	6,302	32,466	5,151
Shanxi	3,243	10,771	3,322	3,292	12,741	3,871
Inner Mong.	4,424	15,353	3,470	5,589	25,285	4,524
Liaoning	3,073	16,601	5,403	3,217	20,705	6,436
Jilin	3,624	23,266	6,420	4,610	33,430	7,251
Heilongjiang	7,778	30,466	3,917	11,520	57,615	5,002
Shanghai	357	2,263	6,332	188	1,213	6,465
Jiangsu	5,877	34,764	5,915	5,337	33,725	6,320
Zhejiang	2,877	15,168	5,272	1,252	7,698	6,151
Anhui	6,028	26,741	4,436	6,622	32,891	4,967
Fujian	2,032	9,522	4,687	1,223	6,593	5,390
Jiangxi	3,570	17,663	4,947	3,676	20,848	5,672
Shandong	8,237	43,327	5,260	7,202	45,114	6,264
Henan	8,964	38,399	4,283	9,985	56,386	5,647
Hubei	4,880	24,844	5,091	4,180	24,418	5,842
Hunan	5,133	27,015	5,263	4,908	30,065	6,126
Guangdong	3,524	18,392	5,219	2,540	13,963	5,497
Guangxi	3,708	15,093	4,071	3,069	14,849	4,838
Hainan	572	1,977	3,459	439	1,995	4,549
Chongqing	-	-	-	2,260	11,385	5,039
Sichuan	10,027	44,957	4,484	6,468	33,150	5,125
Guizhou	2,890	10,126	3,504	3,054	10,795	3,534
Yunnan	3,698	12,462	3,370	4,439	17,491	3,940
Tibet	192	777	4,049	171	950	5,543
Shannxi	4,053	12,173	3,004	3,128	12,451	3,981
Gansu	2,925	8,206	2,805	2,839	11,097	3,908
Qinghai	395	1,238	3,136	280	1,015	3,623
Ningxia	782	2,579	3,299	828	3,750	4,528
Xinjiang	1,661	8,053	4,849	2,131	12,730	5,973
Summary	112,537	504,535	4,483	111,267	589,571	5,299

*: Source from Thematic Database for Human-earth System: http://www.data.ac.cn/index.asp and National Bureau of Statistics, PR China: http://www.stats.gov.cn/english/

Table S7. Data inputs for Van Oost et al.'s (2) and modified methods for calculating F3.

Data Type	Van Oost et al.'s Method		Modified Method	
	Data	Inputs derived	Data	Inputs derived
SOC	Vertical distribution of SOC concentration in stable area.	$C_{T\text{-}NE}$, $c_{top\text{-}t}$ in equation (10) D_{top}, $c_{bel\text{-}(t\text{-}1)}$ in equation (11)	Vertical distribution of SOC concentration in eroded area.	c_{bel} in equation (14) All parameters in equation (16)
	SOC storage in eroded area	$C_{T\text{-}E}$ in equation (10)		
Erosion	Erosion rate	v_{ero} in equation (10)	Erosion rate	k_E, v_{ero} in equation (14)
Area	Eroded area	A_i in equation (12)	Eroded area	A in equation (15)
Time	Length of erosion period	T in equation (12)	From when soil profiles are sampled to any year interested	T in equation (15)
Others			NPP and carbon pool turnover rate	I_B and k_O in equations (13) and (14)

Table S8. Input layers for minimum polygon generation.

Input layers	Data description	Source
National survey of soil erosion in 1995–1996.	370,507 polygons covering the ~9,600,000 km^2 land were divided into six grades of Slight, Light, Moderate, Intense, Extremely Intense, and Severe.	Ministry of Water Resources
National survey of soil erosion in 2010–2012.	Areas of the six grades (Slight, Light, Moderate, Intense, Extremely Intense, and Severe) are given for each of the 2,275 counties in China.	Ministry of Water Resources
National survey of soil organic matter	7,251 soil profiles were sampled at 2–9 layers.	Institute of Soil Sciences, CAS
NPP	Extracted from 10 models (see Table S12) with $1^{o}\times1^{o}$ resolution.	
Turnover rate of soil carbon pool	Extracted from 10 models (see Table S12) with $1^{o}\times1^{o}$ resolution.	

Table S9. ^{137}Cs, carbon inventory of soil profiles, and outputs from Van Oost et al.'s (2) method and present modified method.

Country	T	D_{samp} m	$^{137}Cs_{ref}$ Bq m^{-2}	C_0 g/m^3	k m^{-1}	c_{min}/c_0 -	k_O yr^{-1}	NPP kg/m^2/a	^{137}Cs Bq m^{-2}	SOC g m^{-2}	v_{ero} mm/a	F3-v	F3-m	Ref
Spain	66	0.44	1,870	8,255	5.00	0.004	0.040	0.10	2,316–6,008	2,997/±1,144	3.77	2.5	3.5	(2)
Portugal	66	0.21	1,800	12,399	7.10	0.085	0.040	0.10	2,163–5,351	2,570/±1,058	2.33	5.7	2.8	
UK	55	0.49	2,500	16,562	4.30	0.040	0.020	0.10	2,752–6,200	6,630/±1,098	2.17	5.2	1.9	
Spain	66	0.50	1,870	9,056	5.00	0.050	0.030	0.10	2,264–4,532	3,617/±1,312	3.46	3.2	1.5	
Belgium	80	0.50	3,400	9,161	4.50	0.060	0.040	0.10	4,212–7,403	3,540/±938	2.47	2.4	2.2	
Denmark	68	0.45	2,430	21,808	3.90	0.020	0.010	0.10	2,746–4,321	8,461/±938	2.25	5.2	3.1	
Belgium	100	0.50	3,228	12,225	5.10	0.110	0.030	0.10	3,561–4,430	4,633/±734	1.22	1.6	1.0	
Greece	74	0.20	6,367	8,465	5.40	0.004	0.070	0.10	7,650–12,853	1,728/±428	1.94	0.7	0.6	
USA	143	0.30	2,470	32,040	4.20	0.059	0.010	0.10	332–2,684	9,329/±1,951	2.43	5.7	7.7	
USA	143	0.30	2,470	32,555	4.20	0.059	0.010	0.10	675–2,709	9,480/±1,856	2.20	5.7	6.4	
China	99	0.50	2,377	22,431	0.83	0.001	0.032	0.44	1,052–1,772	9,284–14,251	1.20–3.40	4.4	4.1	(13)
China	70	0.80	-	3,189	5.41	0.420	0.032	0.54	-	1,984	1.75	2.0	1.7	(14)
China	54	0.30	1,769	11,236	4.20	0.001	0.067	0.74	353–1,539	1,400–4,600	0.45–4.35	17.2	17.8	(15)
China	57	0.30	1,259	10,947	4.20	0.001	0.067	0.74	539–1,075	2,200–4,290	0.45–2.25	6.0	4.3	(16)
China	50	0.30	1,113	19,822	3.11	0.001	0.083	0.85	158–938	3,047–6,683	0.45–8.20	16.5	11.9	(17)

D_{samp}: Depth of each sample profile.

$^{137}Cs_{ref}$: ^{137}Cs content in the reference profile of each watershed.

v_{ero}: Erosion velocity.

c_0: SOC content in the surface layer.

k: parameter of vertical distribution of SOC profile, see equation (17).

c_{min}/c_0: parameter of vertical distribution of SOC profile, see equation (17).

k_O: turnover rate of soil carbon.

NPP: Net Primary Product.

F3-v and F3-m: F3 calculated from Van Oost et al.'s and the modified methods. Unit: g C/m^2/yr

Table S10. Validation of CSLE using data from different regions in China

Region	Modeled Erosion Rate (t/hm^2/yr)	Observed Erosion Rate (t/hm^2/yr)	Error (%)	References
North China	10.80	8.00	-25.7	(77)
	13.30	9.90	-25.1	
	48.10	22.00	-54.2	
	24.50	8.80	-64.0	
	42.70	39.80	-6.7	
	21.80	16.40	-24.7	
	5.60	7.10	26.6	
	189.50	240.40	26.8	
	33.00	37.70	14.1	
	49.60	48.70	-1.7	
	73.60	84.30	14.5	
	72.50	64.70	-10.8	
	69.00	80.60	16.8	
South China	53.42	51.95	-2.8	(78)
	0.12	0.12	0.0	
	0.20	0.18	-10.0	
	0.16	0.17	6.3	
	0.06	0.06	0.0	
	0.10	0.09	-10.0	
	25.68	22.59	-12.0	
	0.08	0.09	12.5	
	0.23	0.24	4.3	
	7.32	7.44	1.6	
	0.21	0.22	4.8	
	0.66	0.67	1.5	
Northeast	40.10		-14.7–7.6	(79)
	53.70			
	49.40			
	12.10			
	33.60			
	21.70			
	21.60			
	12.60			
	12.00			
	23.90			
	31.90			
Southwest	2.69	2.56	-4.8	(80)
East China	32.39	16.47–27.45	-15.3–-49.2	(81)

Table S11. Summary of graded areas from National Survey of Soil Erosion in 2010–2012 (29)

Province	Erosion Area (km^2)				
	Light	Moderate	Intense	Extremely Intense	Severe
Beijing	1,746	1,031	341	70	14
Tianjin	108	60	59	6	3
Hebei	22,397	13,087	4,565	1,464	622
Shanxi	26,707	24,172	14,069	4,277	1,058
Inner Mongolia	68,480	20,300	10,118	2,923	577
Liaoning	21,975	12,005	6,456	2,769	783
Jilin	17,297	9,044	4,342	2,777	1,284
Heilongjiang	36,161	18,343	11,657	5,459	1,631
Shanghai	2	2	0	0	0
Jiangsu	2,068	595	367	133	14
Zhejiang	6,929	2,060	582	177	159
Anhui	6,925	4,207	1,953	660	154
Fujian	6,655	3,215	1,615	428	268
Jiangxi	14,896	7,558	3,158	776	109
Shandong	14,926	6,634	3,542	1,727	424
Henan	10,180	7,444	4,028	1,444	368
Hubei	20,732	10,272	3,637	1,573	689
Hunan	19,615	8,687	2,515	1,019	452
Guangdong	8,886	6,925	3,535	1,629	330
Guangxi	22,633	14,395	7,371	4,804	1,334
Hainan	1,171	666	190	45	44
Chongqing	10,644	9,520	5,189	4,356	1,654
Sichuan	48,480	35,854	15,573	9,748	4,765
Guizhou	27,700	16,356	6,012	2,960	2,241
Yuannan	44,876	34,764	15,860	8,963	5,125
Xizang	28,650	23,637	5,929	2,084	1,302
Shaanxi	48,221	2,124	14,679	4,569	1,214
Gansu	30,263	25,455	12,866	5,407	2,121
Qinghai	26,563	10,003	3,858	2,179	202
Ningxia	6,816	4,281	2,065	526	203
Xinjiang	64,895	18,752	2,556	1,320	98
Sum	667,597	351,448	168,687	76,272	29,242

Table S12. Statistics of k_O, NPP and erosion-induced CO_2 fluxes based on parameters derived from ten land carbon models (see References 31–41).

Parameter Source	Average k_O 1/yr	Average NPP kg $C/m^2/yr$	Std. deviation of k_O	Std. deviation of NPP	F3[b] g $C/m^2/yr$	
					1	2
CLM4C	0.04	0.30	0.03	0.32	28.1	29.2
CLM4CN	0.04	0.35	0.03	0.36	40.9	38.0
HYLAND-v4	0.03	0.34	0.03	0.36	55.4	42.5
LPJ	0.03	0.30	0.03	0.25	43.2	34.2
LPJ_GUESS	0.03	0.39	0.03	0.21	55.5	38.6
ORCHIDEE	0.04	0.42	0.02	0.35	64.6	53.2
SDGVM	0.03	0.36	0.03	0.28	50.1	39.2
TRIFFID	-0.03	0.36	0.13	0.46	56.5	52.8
VEGAS-2.1	0.03	0.41	0.02	0.27	62.0	51.4
OCN	0.03	0.34	0.02	0.34	54.7	50.7
Average[a]					51.1	43.0

a: Averaged fluxes calculated from 10 land carbon models.

b: F3(1) is based on the erosion data from the 2nd National Survey in 1995–1996; F3(3) is based on the erosion data from the 4th National Survey in 2010–2012.

Table S13. Summary of parameters used in equations for calculating the five flux components.

Parameter	Carbon Flux	Unit	Description	Equation	Data source
$C_{SOC\text{-}top}$	F1, F3 F4, F5	kg/m^3	Organic carbon content in the top 4.5 cm soil layer	(1), (16) (17), (19)	Organic carbon content in the 1st layer of each soil sample in the Global Soil Dataset.
v_{ero}	F1, F3 F4, F5	m/yr	Erosion rate	(1), (13), (14), (17), (19)	Middle point of the range of erosion rate for each grade.
I_B	F3	$gC/m^2/yr$	Carbon input to the soil	(13), (14)	Mean values of NPP from ten global carbon models.
k_O	F3, F4, F5	1/yr	Turnover rate of soil carbon	(13), (14), (20)	Mean values of k_O from ten global carbon models.
k_E	F3	1/yr	Erosion rate of soil carbon	(14)	Erosion rate, v_{ero}, divided by the depth of soil layer which dominates erosion.
$C_{min}/C_{SOC\text{-}top}$	F3	-	Ratio of organic carbon content in the top layer to that in the bottom layer	(16), (17)	Fit based on SOC profiles from the Global Soil Dataset following the process in Fig. S2.
k	F3	1/m	Attenuation coefficient of SOC profile	(16), (17)	Fit based on SOC profiles from the Global Soil Dataset following the process in Fig. S2.